ORIGINAL ARTICLE

Identifying the Arm Joint Dynamics Using Muscle Synergy Patterns and SVMD-BiGRU Hybrid Mechanism

Seyyed Ali Zendehbad [1], Hamid Reza Kobravi [2*], Mohammad Mahdi Khalilzadeh [1], Athena Sharifi Razavi [3], Payam Sasan Nezhad [4]

[1] *Department of Biomedical Engineering, Mashhad Branch, Islamic Azad University, Mashhad, Iran*

[2] *Research Center of Biomedical Engineering, Mashhad Branch, Islamic Azad University, Mashhad, Iran*

[3] *Clinical Research Development Unit of Bou Ali Sina Hospital, School of Medicine, Mazandaran University of Medical Sciences, Sari, Iran*

[4] *Ghaem Medical Center, Department of Neurology, School of Medicine, Mashhad University of Medical Sciences, Mashhad, Iran*

*Corresponding Author: Hamid Reza Kobravi
Email: hamidrezakobravi@gmail.com

Received: 10 February 2024 / Accepted: 28 July 2024

Abstract

Purpose: In this study, we propose a novel generalizable hybrid underlying mechanism for mapping Human Pose Estimation (HPE) data to muscle synergy patterns, which can be highly efficient in improving visual biofeedback.

Materials and Methods: In the first step, Electromyography (EMG) data from the upper limb muscles of twelve healthy participants are collected and pre-processed, and muscle synergy patterns are extracted from it. Concurrently, kinematic data are detected using the OpenPose model. Through synchronization and normalization, the Successive Variational Mode Decomposition (SVMD) algorithm decomposes synergy control patterns into smaller components. To establish mappings, a custom Bidirectional Gated Recurrent Unit (BiGRU) model is employed. Comparative analysis against popular models validates the efficacy of our approach, revealing the generated trajectory as potentially ideal for visual biofeedback. Remarkably, the combined SVMD-BiGRU model outperforms the alternatives.

Results: The results show that the trajectory generated by the model is potentially suitable for visual biofeedback systems. Remarkably, the combined SVMD-BiGRU model outperforms the alternatives. Furthermore, empirical assessments have demonstrated the adept ability of healthy participants to closely adhere to the trajectory generated by the model output during the test phase.

Conclusion: Ultimately, incorporating this innovative mechanism at the heart of visual biofeedback systems has been revealed to significantly elevate both the quantity and quality of movement.

Keywords: Arm; Electromyography; Joint Dynamics; Muscle Synergy.

DOI:

1. Introduction

The World Health Organization (WHO) highlights the increasing prevalence of functional disabilities due to factors such as aging and neurological diseases, impacting independence and Quality of Life (QOL) and aspects related to Activities of Daily Living (ADL) [1-4]. Neurorehabilitation methods like Exoskeleton robots, Functional Electrical Stimulation (FES), and Biofeedback offer promising avenues for recovery [5-9]. Biofeedback, particularly EMG-based, influences brain neuroplasticity and has shown promise in post-stroke rehabilitation [10, 11]. Various studies explore the efficacy of auditory, visual, and EMG biofeedback in improving motor function post-stroke [12-27]. EMG signals offer distinct advantages for biofeedback due to their ability to convey muscle activation patterns [28-31]. However, challenges persist in optimizing visual biofeedback trajectories and addressing the variability in muscle activity across individuals [32-37]. Recent research incorporates Deep Learning (DL) strategies, including Convolutional Neural Networks (CNN) and Recurrent Neural Networks (RNN), to enhance accuracy and robustness [38-44]. Understanding the intrinsic properties of EMG signals, such as non-stationarity and susceptibility to noise, is crucial for accurate analysis and interpretation [45-50]. Methods like Empirical Mode Decomposition (EMD) and Variable Mode Decomposition (VMD), along with novel approaches like Sequential Variable Mode Decomposition (SVMD), offer solutions for signal processing challenges [51-56]. The paper introduces the SVMD-BiGRU method, aiming to map kinematic data to muscle synergy, presenting a promising direction for future research. The following summarizes the contribution of this research:

• Overcoming challenges in traditional approaches, addressing issues like marginal effects and mode confusion in EMD, and eliminating the need to determine the number of modes in VMD or decompositions in the EMD method.

• Adeptly decomposing EMG data, revealing hidden patterns in time series data, and showcasing the model's ability to predict data without relying on previous information or parametric assumptions.

• Demonstrating exceptional versatility, the model proves effective for various EMG and HPE data streams related to both upper and lower extremities.

• Experimental results highlight superior performance and faster execution compared to conventional methods, positioning the SVMD-BiGRU method as an ideal choice for biofeedback applications.

• The usability of the visual trajectory generated based on the proposed model was evaluated by healthy subjects, and it was confirmed to be user-friendly.

The remainder of this paper is organized as follows. Section 2 introduces the data collection, adopted methodology, and constructs the proposed hybrid model based on the presented method. Experimental results are shown in Section 3, the discussion is shown in Section 4, and Section 5 gives the conclusions, limitations, and suggestions for future research.

2. Materials and Methods

2.1. Data Collection

In this study, twelve individuals in a healthy condition (comprising eight males and four females, ranging from 21 to 63 years of age, all right-handed) and devoid of any medical history or skeletal disorders actively participated in the experiment. The number of samples was selected based on statistical power analysis and comparable research, which shows that this sample size is sufficient to detect significant effects in our proposed model. The homogeneity of the sample increases the reliability of the data and makes it suitable for our study. Thus, all participants were right-handed and devoid of medical issues.

Before any data collection, the participants were informed, and a permission form was signed. The study protocols were clear for all the Participants. The Ethics Committees and the Iranian Registry of Clinical Trials (IRCT) approved this study [57]. The participants had no history of musculoskeletal disorders or cognitive problems. The demographic characteristics of the participants are illustrated in Table 1.

During the experiment, participants remained seated with the visual monitor positioned nearby, within a meter's distance. They performed horizontal movements with internal rotation using their right hand. Electrodes were placed on the Posterior Deltoid (PD), Pectoralis Major (PM), Middle Trapezius (MT), and Lower Trapezius (LT) muscles, following

Table 1. Demographic characteristics of healty participants

Parameters		The Participants (N =12) (Mean±SD)
Age (years)		41.55± 16.23
Gender	Female	3(25%)
	Male	9(75%)

Abbreviations: Values are expressed as Mean ± Standard Deviation

SENIAM and electromyography guidelines, with a consistent electrode spacing of 20 mm [57]. Challenges such as loose skin, hair, fat, sweat, and coldness can affect signal quality and electrode adhesion [58]. Table 2 describes the approximate location of the electrodes for each muscle.

Table 2. Placement of electrodes for each muscle [57-58]

Channel	Muscles	Position	References
1	Posterior Deltoid (PD)	2 cm below posterior crista of the scapular acromion.	SENIAM guidelines [57]
2	Pectoralis Major (PM)	3 cm below the one-third line from the medial clavicular head to the scapular acromion.	
3	Middle Trapezius (MT)	The middle point on the horizontal line between the root of the scapular spine and the third thoracic spine.	D.C. Preston and B.E. Shapiro [58]
4	Lower Trapezius (LT)	The Middle point between the spinous process of the seventh cervical vertebra and the trigonum scapula.	

Surface EMG signals were recorded with electrodes placed on muscle bellies after skin exfoliation and cleansing, with reference electrodes on the thoracic spine bone [58]. A commercial Flex-Comp Infiniti amplifier was used, sampling at 2048 Hz. Participants performed shoulder movements, aiming to adjust speed based on visual and audio feedback. Movements included internal and external rotation within the accepted range of 0° to 90°. Data collection comprised five rapid movements lasting 10 seconds each and three slower movements lasting 20 seconds each, with a 10-second break between fast and slow movements to prevent fatigue. To improve the model's performance, we first implemented several conventional pre-processing steps. Initially, a bandpass Butterworth filter with cut-off frequencies between 40-400 Hz was used. A low cut-off frequency of 40 Hz was selected to remove low-frequency components, including motion artifacts and baseline drift, which are common in EMG recordings. A cut-off frequency above 400 Hz was selected to eliminate high-frequency noise and electrical interference and ensure that the signals related to muscle activity were preserved concerning its frequency range. All negative signal values were then corrected to positive, which is necessary to create a clear representation of the signal amplitude. Outliers were removed to increase signal reliability by removing outliers that could confound the analysis. After that, a low-pass filter with a cut-off frequency of 4 Hz was applied to obtain the EMG envelopes. This step was critical for smoothing the rectified EMG signals, highlighting the overall muscle activation pattern while reducing high-frequency noise. The choice of 4 Hz was based on its effectiveness in capturing the envelope of muscle activity, which typically exhibits low-frequency characteristics [38]. The pre-processing steps are shown in Figure 1. For joint position analysis, an HD webcam was used, with OpenPose chosen for Human Pose Estimation (HPE) due to its effectiveness in managing multiple individuals and crowded scenes [59-62]. The selection of OpenPose for HPE is justified due to its strong ability to manage complex movements. OpenPose is highly effective in detecting and tracking multiple body parts and joints with precision, even in dynamic and cluttered settings. Its

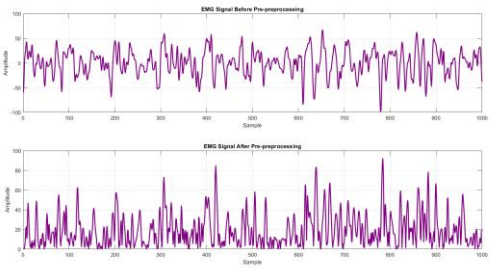

Figure 1. EMG signal display after pre-processing steps

capability to handle multi-person detection and accurately estimate key points makes it ideal for real-time applications involving intricate human movements [63, 64].

In our study, depicted in Figure 2, we have selected key points 1 through 7 for the upper limb. It's noteworthy that these points necessitated robust synchronization due to the frequency variance observed in the input data [65, 66].

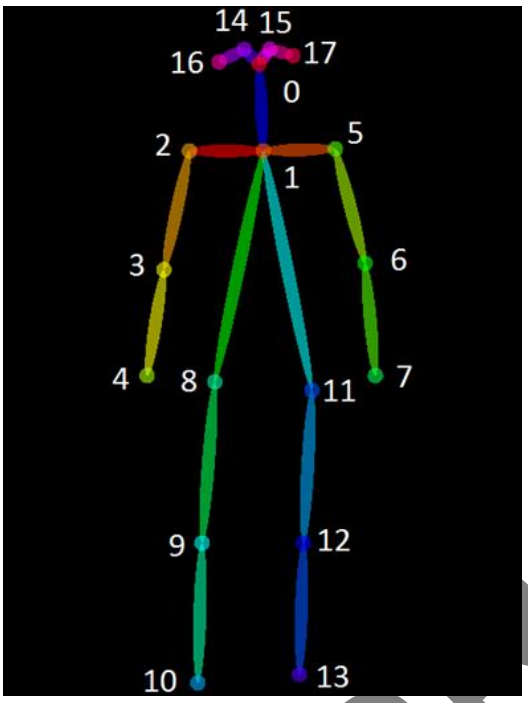

Figure 2. OpenPose key points topology [65-66]

A down sampling technique aligned the EMG signal (2048 Hz) with pose estimation processing (around 30 Hz), achieving effective synchronization. Signal normalization using the min-max approach enhanced performance outcomes. Vectorization of both signals ensured compatibility in dimensions for network integration, facilitated by the Numpy Library, boosting processing speed.

2.2. The Proposed Methodology

The study introduced a two-phase model to address the challenges discussed earlier. In the offline stage, as depicted in Figure 2a, the data underwent pre-processing, and the muscle synergy control matrices were derived using the HALS algorithm. Concurrently, OpenPose estimated joint positions relevant to arm movement. The pre-processing step involved synchronization and normalization based on a dynamic function adaptable to varying frequency rates via a down-sampling method. To enhance patient understanding, three synergy control matrices were transformed into a time series using an averaging block. In addition, the SVMD method facilitated the simultaneous decomposition of all EMG pattern modes, emphasizing compactness around a central frequency. Now, each of these extracted modes as input $h(t)$ and kinematic data as input $x(t)$ is entered into the Bi-GRU model for prediction and training. The model's output for each mode was summed for the final prediction. According to Figure 3b, in the online phase and without EMG recording, assisted by the trained model developed during the offline phase, it can be used by comparing $h(t)$ (desired trajectory) and $\hat{h}(t)$ (actual trajectory) as an underlying mechanism based on muscle synergy to develop visual biofeedback systems.

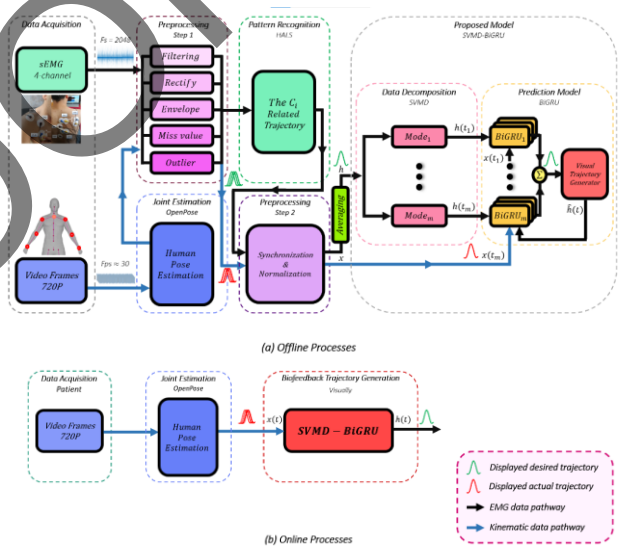

Figure 3. Block diagram illustrating the proposed model in (a) offline (train) and (b) online (test) modes

A. Extracting the Muscle Synergy Pattern

For each movement, muscle patterns are a linear combination of time-varying synergies or coordinated activations of a group of muscles with a specified onset time and varied intensity course. Each muscle synergy includes a weight coefficient, amplitude range, and time shift [67]. The muscle activation pattern was created by combining these synergies. The time-varying synergy model can be defined as Equation 1 [68].

$$M(t) = \sum_{i=1}^{N} C_i W_i (t - t_i) \quad (1)$$

Where M is the pattern of time-varying muscle activity, the number of time-varying synergies is denoted by N, for the ith synergy, C_i is a non-negative scaling coefficient called the control matrix, and t_i is the synergy onset delay, W_i is the weighting matrix, which is the muscle activity for ith synergy at the time t_i. Because muscle activation is a nonnegative quantity, C and W are nonnegative. Several approaches for obtaining C and W coefficients have been proposed. HALS are well suited for our technique. HALS provides a broad range of capabilities, and is computationally cheaper than the conventional NMF method, and can work with many different components [68]. Finally, the following HALS algorithm was used to extract the synergetic patterns of shoulder movement:

$$M = [W][C]^T \quad (2)$$

Consider a preprocessed set of EMG signals denoted as M, organized in an m by n matrix, where m represents the number of time series and n is the count of EMG channel inputs. Let $C = [c1,..., c_j]$ be the synergy set, where j corresponds to the number of synergies, and $c_j = [c1, \ldots, c_n]^T$ represents an individual set of synergies. Here, c_n signifies the coactivation coefficient of EMG n. Additionally, W is the coactivation coefficient of the synergy, presented as a matrix with dimensions m by j [69]. Once the synergy model is developed, learning algorithm approaches are used to iterate Equation 3 and Equation 4 several times, with k (1, 2,..., j) denoting the label of synergies [69]. C and W matrices were generated using a single set of shoulder movement EMG data.

$$[C_k] \leftarrow [C_k] + \frac{([M][W]^T - [C][W]W^T)_K}{[W_k][W_k]^T} \quad (3)$$

$$[W_k] \leftarrow [W_k]^T + \frac{([M]^T[C] - [W]^T[C]^T[C])_K}{[C_k]^T[C_k]} \quad (4)$$

B. The Proposed Hybrid Model

The architecture of the proposed hybrid model is illustrated in Figure 2. It shows that the synergy patterns are inputs of the model and visual biofeedback trajectory is the model output. First, a decomposition method is used to decompos synergy control patterns into smaller components. The Successive Variational Mode Decomposition (SVMD) proves advantageous in EMG data decomposition, offering a systematic approach that ensures accuracy and robustness to noise [54]. Its efficiency in real-time applications, coupled with its adaptability to dynamic signals, makes SVMD a valuable tool for unraveling complex EMG data nuances. Similarly, VMD, based on the Wiener Filter and Hilbert Transform, employs an iterative framework to extract optimal results, decomposing EMG signals into discrete sub-signals with limited bandwidth [53]. This iterative process continues until all modes are extracted or the reconstruction error falls below a predefined threshold [54]. But the process of the SVMD algorithm is as follows:

- **Step 1**. Initialization of parameters.
- **Step 2**. By using Parswal's equality applying some change of variables and expanding the equations with new variables, as well as using the Alternating Direction Method of the Multiplier algorithm (ADMM) to repeatedly solve the minimization problem and calculate $\hat{u}_L^{n+1}(\omega)$.
- **Step 3**. Update ω_L^{n+1}.
- **Step 4**. Using the double ascent approach, the updated equation of the Lagrangian multiplier $\hat{\lambda}^{n+1}(\omega)$ is calculated.
- **Step 5**. The algorithm is repeated until the convergence condition [54].

After decomposing, the extracted Intrinsic Mode Function (IMF), as the input data, was given to the Artificial Neural Network (ANN). The used ANN was a Bidirectional Gated Recurrent Unit (BiGRU). This ANN will be elaborated on in the next subsection. In summary, the SVMD-BiGRU method is as follows:

- **SVMD Decomposition:** Utilizes the SVMD approach with parameters such as Number Of Modal (NOM), α_{min}, $\alpha_{max}, \tau,$ and ε to decompose control synergy data into modal subsets.
- **Mode Period Calculation:** Determines the period of each mode component by evaluating the ratio

of sample points to local extrema (maxima or minima) within each subset.

BiGRU Prediction: Applies a dedicated BiGRU model to predict x_t, input based on each mode subset represented by h_t, generating individual prediction results.

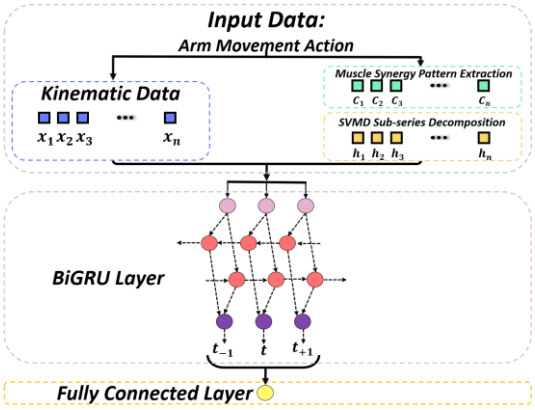

Figure 4. Architectural structure of the SVMD–BiGRU model

- **Prediction Combination:** Integrates predictions from all mode subsets to produce the final prediction outcome.
- **Input Dataset Reconfiguration:** Reorganizes the input dataset into a time loop window spanning from time $t+1$ to time $t-1$ to facilitate sequential processing and prediction continuity.
- **BiGRU Model Application:** The restructured input dataset is fed into the BiGRU model, which consists of four hidden layers followed by a Fully Connected (FC) layer. This configuration enables the model to predict the human pose accurately at time t based on the processed input data.

It was explained previously that the SVMD was used to decompose the input data $h(t) = \{h_1, h_2, \ldots, h_n\}$, into $Mode = \{mode_j\}, j = 1, \ldots, NOM,$. Then, we use the BiGRU approach to predict each $mode_j, j = 1, \ldots, m$ and get the predicted value based on $x(t) = \{x_1, x_2, \ldots, x_n\}$ of each mode as follows (Equation 5):

$$O_j = BiGRU(mode_j), j = 1, \ldots, NOM \quad (5)$$

After obtaining the predicted value O_j of each $mode_j$, the final result is expressed as:

$$Fh = \sum_{j=1}^{NOM} (O_j) \quad (6)$$

Where O_j represents the predicted value of $mode_j$, because $h = \sum(mode_j)$, the predicted value of h is shown in Equation 6.

It is worth noting that selecting suitable initial values for SVMD is essential for the effective denoising of sEMG signals. Therefore, NOM is usually selected in the range of 5 to 10, and according to the frequency range of sEMG, it creates a balance between analysis granularity and computational efficiency, which was selected in this study as 12. The regularization parameter (λ) should initially be set to a small positive value (0.1 to 1) to achieve a trade-off between preserving signal fidelity and ensuring smoothness. The threshold parameter (O_j) needs to be dynamically adapted based on the standard deviation of each Intrinsic Mode Function (IMF). Additionally, the BiGRU architecture in this study includes two hidden layers, each comprising 128 neurons, optimized with the Adam optimizer set at a learning rate of 0.001. A batch size of 32 is used, along with a dropout rate of 0.3 to prevent overfitting. The update and reset gates use a sigmoid activation function, while the candidate activation uses a hyperbolic tangent function. The model is trained for 50 epochs, with Xavier initialization for weights and L2 set to 0.01. The input sequences have a length of 30-time steps, balancing computational efficiency and the ability of the model to capture temporal dependencies in EMG signals.

C. The Adopted Neural Network

Generally, a time series is a collection of vectors that are dependent on time t. The ability to predict the future values of a vector called y is useful or essential when deciding on a control plan or optimizing activity, production, or selection [70]. The issue of prediction can be formalized as finding a function that yields an estimate $\hat{y}\ (t+D)$ of the vector y at time $t+D$ $(D = 1,2,3,\cdots)$, given the values of y up to time t, plus some time-independent variables (exogenous features) u_i (Equations 7, 8):

$$y(t), t = 0, 1, 2, \ldots \quad (7)$$

$$\hat{y}(t+D) = f\left(y(t), \cdots, y(t-d_y), x(t), \cdots, x(t-d_u)\right) \quad (8)$$

where $x(t)$ and $y(t)$ are the model's input and output at time t, dx, and dy are the system's input and output delays, respectively; and f is a nonlinear function. D is usually set to 1, indicating one step forward, but it may be set to any number greater than one (multi-step-ahead) [71]. Among all the proposed structures, RNNs are capable of modeling arbitrary nonlinear dynamic systems [72]. Unlike traditional feed-forward neural networks, RNNs maintain a state that allows them to anticipate information from any past window [73, 74]. Schuster *et al.* proposed a bidirectional RNN able to use forward and backward information [75]. The GRU architecture was first introduced by Chung *et al.* in 2014 to solve the traditional recurrent neural network problems such as the vanishing gradient problem or reducing the parameters in the LSTM architecture [76]. This study replaces traditional RNN cells with GRUs. Using the BiGRU, two hidden layers with opposite transmission directions are connected to the same output layer and provide information on past and future states. This means, the BiGRU neural network can make more accurate predictions since it can learn information from two different directions. A BiGRU splits the regular GRU neurons into forward and backward states (positive and negative time directions) [77]. Figure 5 illustrates the general BiGRU structure.

As illustrated in Figure 6, the GRU cell has two gates, including an update gate z_t and a reset gate r_t [78]. The update gate z_t controls the amount of new information from the input data to the current state. the larger z_t is, the more additional information we will have from the input data. The function of the reset gate r_t controls the amount of ignoring the status information related to the previous time. the smaller r_t is, the more previous status information is ignored. At time t, x_t denotes the input and h_t denotes the hidden state. The symbol $\otimes$ is the element-wise multiplication and $\tilde{h}_t$ which is the candidate vector

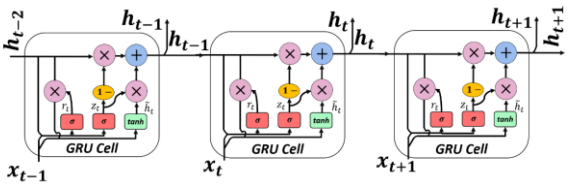

Figure 5. Interaction structure of GRU cells [81]

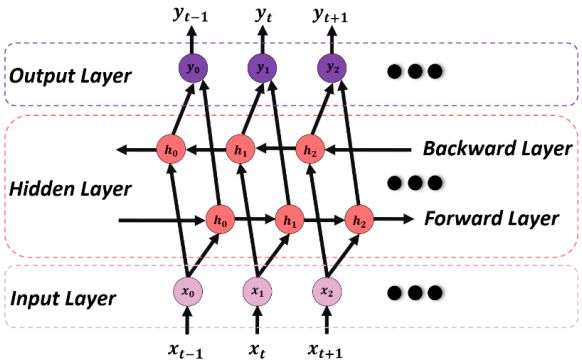

Figure 6. Overview of BiGRU network structure [81]

that controls the rate of receiving new input information in the cell state during a modulation operation. σ denotes the sigmoid function, and $tanh$ is the hyperbolic tangent function. The update gate z_t and the reset gate r_t are calculated as illustrated in Equation 9, where W_r, W_z, and $W_{\tilde{h}_t}$ represent weight matrices. [ ] indicates that the two vectors are connected to each other, and $*$ denotes the element-wise multiplication [78].

$$\begin{aligned} r_t &= \sigma\left(W_r . [h_{t-1}, x_t]\right) \\ z_t &= \sigma\left(W_z . [h_{t-1}, x_t]\right) \\ \tilde{h}_t &= tanh\left(W_{\tilde{h}_t} . [r_t * h_{t-1}, x_t]\right) \\ h_t &= (1 - z_t) * h_{t-1} + z_t * \tilde{h}_t \\ y_t &= \sigma(W_o . h_t) \end{aligned} \quad (9)$$

As discussed, The BiGRU model includes two 128-neuron hidden layers, optimized with the Adam optimizer (learning rate 0.001), a batch size of 32, and a dropout rate of 0.3

3. Results

3.1. Implementation Details

All models and methods were done using a Personal Computer (PC) running Windows 10 64bit, with 32GB RAM, intel Core i7 - 12700k, and an NVIDIA RTX 2070 with 16GB of VRAM. For the software part, we used Python 3.9 with OpenCV, TensorFlow, Numpy, and Pytorch for DL models and calculations. MATLAB 2023a was also used for some pre-processing of label data in text format to have a better understanding of the data. The data for training the reference model was divided into training and testing sets, with 80% of the data allocated for training and 20% for testing.

3.2. Performance Criteria

To evaluate the results of muscle synergy extraction, we used R^2 and, Mean Square Error (MSE). In order to enhance comprehension of the output produced by the HALS algorithm, we used R^2. Using R^2 we can determine the number of synergy matrixes. In Equation 10, the term SSE denotes the sum of squared residuals, and SST is the sum of the remaining squares computed from the mean activation vector ($\bar{m}$) [79].

$$R^2 = 1 - \frac{SSE}{SST} = 1 - \frac{\sum_s \sum_{k=1}^{k_s} \|m^s(t_k) - \sum_i c_i^s w_i (t_k - t_i^s)\|^2}{\sum_s \sum_{k=1}^{k_s} \|m^s(t_k) - \bar{m}\|^2} = 1 - \frac{\sum_{t=1}^{N} (\tilde{h}_t - h_t)^2}{\sum_{t=1}^{N} (\bar{h}_t - h_t)^2} \quad (10)$$

Using the MSE as a loss function, BiGRU evaluated the accuracy of the models. Equation 11 was used to calculate the MSE loss function

$$MSE = \frac{1}{N} \sum_{i=1}^{N} \left(\hat{h}(t) - h(t)\right)^2 \quad (11)$$

For evaluating the goodness of fit of the proposed model, four measurement indexes were established to assess its validity: Root Mean Square Error (RMSE), Mean Absolute Percentage Error (MAPE), and Coefficient of determination (R^2), whose formulas are as follows (Equation 12, 13):

$$RMSE = \sqrt{\frac{1}{N} \sum_{i=1}^{N} (\tilde{h}_t - h_t)^2} \quad (12)$$

$$MAPE = \frac{1}{N} \sum_{i=1}^{N} \left| \frac{\tilde{h}_t - h_t}{h_t} \right| \quad (13)$$

Where $\tilde{h}_t$ and h_t are the predicted value and the actual value at the time t, respectively, $\bar{h}_t$ is the average of the actual value, and N is the total number of samples. To quantify the tracking quality, we computed the Correlation Coefficient (CC) between the displayed actual trajectory and the desired trajectory. Assume that we have two time-series observations, H (Actual trajectory) and R (Desired trajectory) of length n. Pearson's correlation coefficient between the two time-series can be computed as follows:

$$H = h_1, h_2, \cdots, h_i, \cdots, h_n$$
$$R = r_1, r_2, \cdots, r_i, \cdots, r_n$$
$$CC(H,R) = \frac{\sum (h_i - \bar{h})(r_i - \bar{r})}{\sqrt{\sum (h_i - \bar{h})^2 \sum (r_i - \bar{r})^2}} \quad (14)$$

3.3. Quantitative Results

We conducted recordings of muscle activations from four sources and applied the HALS algorithm to extract three muscle synergy matrices. The R^2 value remained consistently stable, indicating synergies exceeding 2. The variations in R^2 concerning the number of both Figure and Figure 8. Additionally, Figure 9 presents the mean MSE values during the reconstruction of muscle activation patterns using the extracted C and W synergy matrices. The resultant model is deemed acceptable, given the mean MSE of 0.0037. Notably, considering the range of the extracted muscle activation pattern (0-1), the computed MSE is notably low relative to the data range, suggesting commendable reconstruction performance.

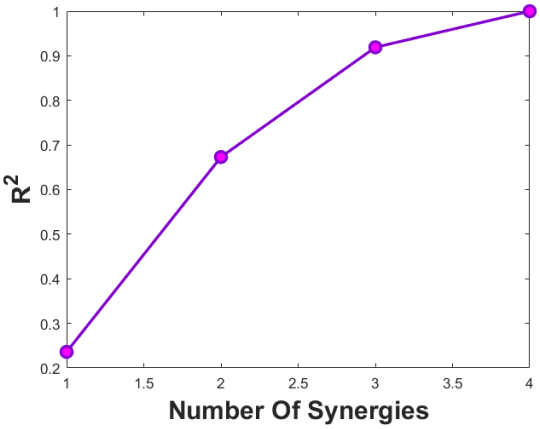

Figure 7. The average R^2 value calculated in connection to the quantity of synergy matrices

The prediction results encompass two key aspects. Firstly, a comparative analysis was carried out, assessing the performance of the proposed model against established conventional models such as NARX, LSTM, GRU, BiLSTM, and BiGRU, specifically in terms of mapping synergistic patterns to kinematic data. Secondly, the trajectory tracking

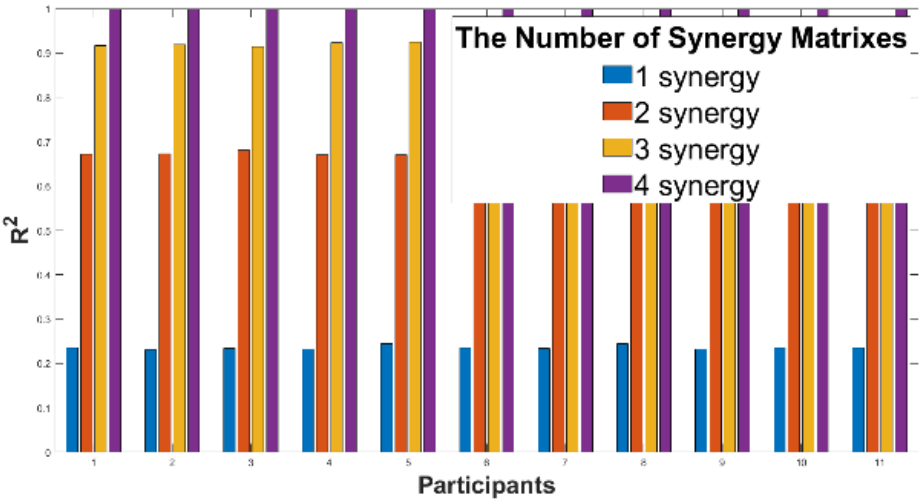

Figure 8. Variations in the R^2 index among participants and the overall mean with respect to the number of synergy matrices

designed by the proposed model will be evaluated in dynamic scenarios with two different speeds on healthy participants. As can be seen in Table 3 and Table 4 The performance evaluation of different methods for healthy participants, the models have varied performances in the evaluation indices compared to each other. Figure 10 and Figure 11 illustrate the outputs of both conventional models and the proposed model across five samples.

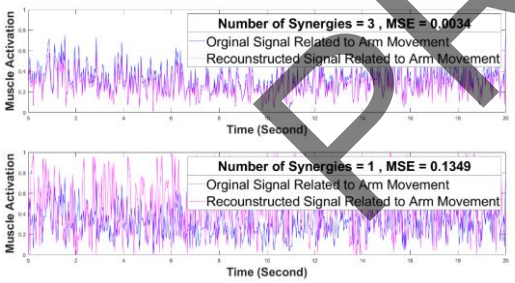

Figure 9. The participant (AZ) exhibits muscle activation patterns, and the obtained reconstructed signals are associated with two distinct numbers of muscle synergy patterns

Table 4. The performance evaluation of different methods for slow movement

Method	RMSE	MAPE (%)	R^2
NARX	0.1353	33.32	0.86
LSTM	0.1655	40.73	0.80
GRU	0.1216	29.78	0.89
BiLSTM	0.1567	38.50	0.82
BiGRU	0.1038	25.49	0.92
SVMD- BiGRU	0.0999	24.48	0.93

Table 3. The performance evaluation of different methods for fast movement

Method	RMSE	MAPE (%)	R^2
NARX	0.1485	36.57	0.84
LSTM	0.1887	40.30	0.74
GRU	0.1408	34.67	0.85
BiLSTM	0.1728	42.52	0.78
BiGRU	0.1171	28.79	0.90
SVMD- BiGRU	0.1044	25.63	0.92

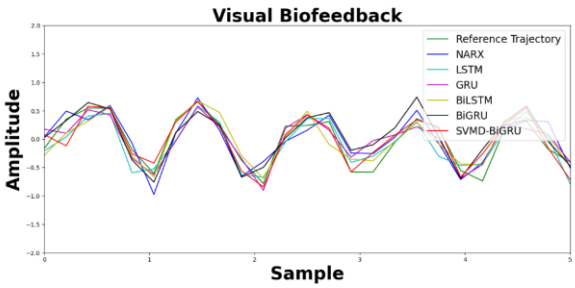

Figure 10. Comparison of fast movement output results from different models

Figure 12 illustrates the SVMD decomposition results of synergistic control patterns for slow and fast motion. This decomposition reveals 12 modes ranging from low to high frequencies, labeled as M1, M2, ..., and M12. M1 represents the lowest frequency signal of sequences, reflecting the long-term activity of the involved muscles, while M12 represents the highest hidden frequency component in the original signal, containing detailed information about the muscles

involved in movement. The analysis results for two-speed movement show that the analyzed modes of SVMD follow a specific pattern.

The original signal spectrum offers a holistic view of the signal's frequency content, revealing dominant frequencies and periodicities [80]. In contrast, the reconstructed signal spectrum post-SVMD decomposition provides a detailed breakdown of individual modes, each representing a distinct oscillatory pattern extracted from the original signal [56]. Analyzing these modes' spectra allows for a nuanced understanding of specific frequency components associated with different behaviors or phenomena in the signal.

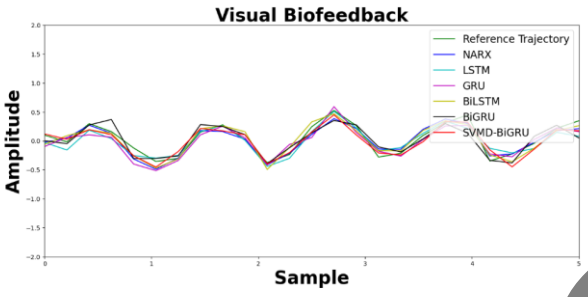

Figure 11. Comparison of slow movement output results from different models

Figure 12. The SVMD decomposition reveals two distinct patterns: (up) corresponding to slow movement and (down) indicative of fast movement

Figure 13 provides a comprehensive visualization encompassing the Input Signal, Reconstructed Signal,

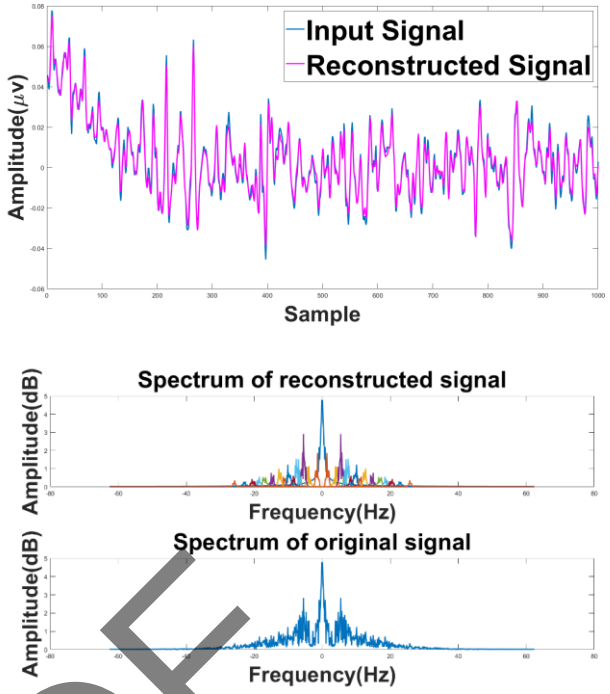

Figure 13. SVMD decomposition results: (up) shows the input signal and the reconstructed signal, and (down) shows the original signal spectrum as well as the spectrum of the reconstructed signal

and spectral analyses of both the original and reconstructed signals. This representation offers a holistic perspective on the signal decomposition process and the corresponding spectral characteristics.

3.4. Qualitative Results

The study aimed to evaluate the trackability of a visual biofeedback trajectory designed for arm movement rehabilitation. Participants were tasked with aligning their arm movements with a displayed trajectory, representing the desired biofeedback signal. The effectiveness of the trajectory was assessed by participants' ability to accurately follow it, indirectly adjusting disturbed muscular synergy patterns. Figure 14 illustrates a participant's attempt to track the trajectory, highlighting the study's focus on participant engagement and biofeedback effects. Figure 15 and Table 5 show the result of the tracking analysis. The mean and standard deviation of the calculated values of CC are 0.911 and 0.040, respectively. These values could convince us that the designed trajectory was trackable by the participants. Despite the dynamic changes in the displayed trajectory's geometry, participants demonstrated the ability to generate a motion-related trajectory that

maintained an acceptably strong correlation with the reference trajectory. Last, in the evaluation of the ease of use of our recently created visual biofeedback plan, a Likert scale survey was given to 12 healthy volunteers. The survey included comments covering different areas of the user experience, with participants giving scores on a scale from 1 (Strongly Oppose) to 5 (Strongly Approve). The volunteers assessed factors like the simplicity of the interface, simplicity of tracking, clarity of visual signals, and the general ease of use of the system [81].

Figure 14. A participant is seated in front of a monitor and is trying to track the displayed visual feedback trajectory

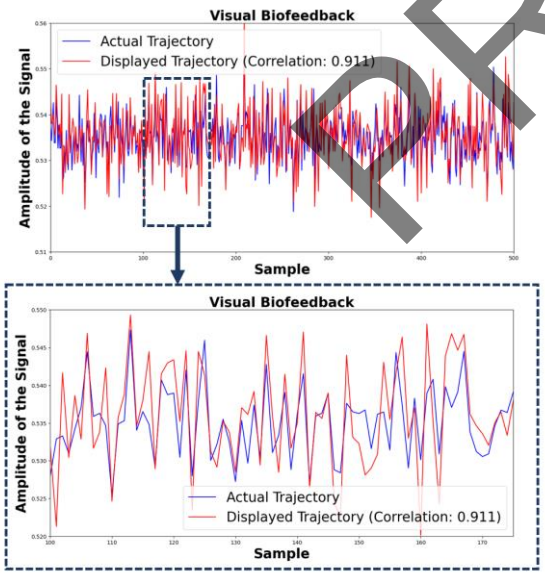

Figure 15. Tracking accuracy assessment for one participant abbreviated as BK

Table 5. The mean value of the computed CC for each participant

Participant ID	Correlation Coefficient (CC)
AZ	**0.933**
ZS	**0.916**
MP	**0.865**
HD	**0.967**
KA	**0.906**
MS	**0.860**
MR	**0.938**
HR	**0.974**
BK	**0.911**
OA	**0.826**
AT	**0.913**
MR	**0.900**

4. Discussion

Integrating EMG biofeedback into neurorehabilitation poses challenges in designing effective feedback signals [82]. This study aimed to propose a mechanism for generating kinematic-related trajectories from muscle synergy patterns and assess their trackability by healthy participants [83]. Muscle synergy's adaptability in healthy individuals contributes to motor action flexibility. However, potential limitations include the small sample size of healthy participants, limited sample diversity, and the involvement of a restricted number of muscles in movement. Furthermore, there is a critical need for clinical trials and broader studies involving patient populations rather than relying solely on synergy pattern extraction from healthy participants. These factors could affect the generalizability of the study's findings to diverse clinical contexts. However, our central hypothesis was formed based on human motor control, which states that these movement patterns are common among all people for voluntary movements [84]. Positive feedback from user-friendliness assessment affirms the model's design. Such findings provide encouraging insights before patient testing. Synergy analysis suggests potential generalizability in arm movement patterns [85]. Challenges in adjusting model hyperparameters due to non-stationary biological data are noted, necessitating iterative refinement. Table 3, Table 4, Figure 10, and Figure 11 that the performance of SVMD- BiGRU compared model has less error and better performance than other models.

The study highlights the advantages of the SVMD-BiGRU model over classical recurrent neural networks,

emphasizing its ability to avoid issues like vanishing or exploding gradients while requiring fewer parameters compared to LSTM [86, 87]. This superiority is attributed to BiGRU's bidirectional architecture, which effectively mitigates issues such as vanishing or exploding gradients while requiring fewer parameters compared to LSTM models. The bidirectional design enables BiGRU to concurrently assimilate information from past and future contexts, thereby enhancing its proficiency in understanding and predicting sequential patterns [88]. Furthermore, the model's capability to accurately track slow and fast movements aligns with dynamic biological system dynamics, affirming its robustness in practical rehabilitation scenarios. The integration of SVMD with BiGRU proves effective, significantly enhancing performance with non-stationary data like EMG, thereby showing promising applications in visual biofeedback-based rehabilitation systems. This study represents a crucial advancement towards developing adaptive rehabilitation technologies capable of personalized treatment approaches.

5. Conclusion

The study addresses the gap in understanding the design of visual biofeedback signals for arm movement recovery applications, focusing on muscle activity patterns. By employing the SVMD-BiGRU model, it generates a kinematically related trajectory. Results show superior performance of the SVMD-BiGRU model compared to conventional ones, and healthy subjects found the trajectory user-friendly and trackable. The approach discussed holds promise for developing neurorehabilitation strategies using visual biofeedback for upper limb paralysis patients. Future work includes conducting clinical trials to evaluate efficacy in real-world settings, longitudinal studies for assessing long-term benefits, and refining the biofeedback system for personalized patient use.

Acknowledgments

Our special thanks go to the Scientific Core of Robotic Rehabilitation and Biofeedback of Mashhad Azad University, the Department of Neurology, and Boualicina Hospital, Sari, Iran. We express our gratitude to the participants who patiently participated in this study. We also thank www.grammarly.com text editing service for assisting us in enhancing the grammar and writing quality of this manuscript.

This study was approved by the Ethics Committees at Mazandaran University of Medical Sciences (IR.MAZUMS.REC.1398.902) and the Iranian Registry of Clinical Trials (IRCT20200914048720N1).

References

1- World Health Organization, Global report on health equity for persons with disabilities. *World Health Organization*, (2022).

2- Hojjat Allah Haghgoo, Elmira Saed Pazuki, Ali S Hosseini, and Mehdi Rassafiani, "Depression, activities of daily living and quality of life in patients with stroke." *Journal of the neurological sciences*, Vol. 328 (No. 1-2), pp. 87-91, (2013).

3- Neilzo Nunes Oliveira, Érica Midori Ikegami, Nayara Gomes Nunes Oliveira, and Darlene Mara dos Santos Tavares, "Factors associated with functional disability in older adults with cataract: integrative review." *Revista Brasileira de Geriatria e Gerontologia*, Vol. 24p. e220076, (2022).

4- William D Spector and John A Fleishman, "Combining activities of daily living with instrumental activities of daily living to measure functional disability." *The Journals of Gerontology Series B: Psychological Sciences and Social Sciences*, Vol. 53 (No. 1), pp. S46-S57, (1998).

5- John W Krakauer, "Motor learning: its relevance to stroke recovery and neurorehabilitation." *Current opinion in neurology*, Vol. 19 (No. 1), pp. 84-90, (2006).

6- Julie Moreland and Mary Ann Thomson, "Efficacy of electromyographic biofeedback compared with conventional physical therapy for upper-extremity function in patients following stroke: a research overview and meta-analysis." *Physical therapy*, Vol. 74 (No. 6), pp. 534-43, (1994).

7- Ana Cisnal, Paula Gordaliza, Javier Pérez Turiel, and Juan Carlos Fraile, "Interaction with a hand rehabilitation exoskeleton in EMG-driven bilateral therapy: Influence of visual biofeedback on the users' performance." *Sensors*, Vol. 23 (No. 4), p. 2048, (2023).

8- Yukihiro Hara, "Neurorehabilitation with new functional electrical stimulation for hemiparetic upper extremity in stroke patients." *Journal of Nippon Medical School*, Vol. 75 (No. 1), pp. 4-14, (2008).

9- Lonnie A Nelson, "The role of biofeedback in stroke rehabilitation: past and future directions." *Topics in stroke rehabilitation*, Vol. 14 (No. 4), pp. 59-66, (2007).

10- Aaron R Seitz, "Cognitive neuroscience: targeting neuroplasticity with neural decoding and biofeedback." *Current Biology*, Vol. 23 (No. 5), pp. R210-R12, (2013).

11- Sisi Feng *et al.*, "EMG biofeedback combined with rehabilitation training may be the best physical therapy for

improving upper limb motor function and relieving pain in patients with the post-stroke shoulder-hand syndrome: a Bayesian network meta-analysis." *Frontiers in Neurology*, Vol. 13p. 1056156, (2023).

12- He Huang, Steven L Wolf, and Jiping He, "Recent developments in biofeedback for neuromotor rehabilitation." *Journal of neuroengineering and rehabilitation*, Vol. 3pp. 1-12, (2006).

13- Robert Teasell *et al.*, "Developing a framework for utilizing adjunct rehabilitation therapies in motor recovery of upper extremity post stroke." *Topics in Stroke Rehabilitation*, Vol. 30 (No. 5), pp. 493-500, (2023).

14- Oonagh M Giggins, Ulrik McCarthy Persson, and Brian Caulfield, "Biofeedback in rehabilitation." *Journal of neuroengineering and rehabilitation*, Vol. 10pp. 1-11, (2013).

15- Sophie Hall, Fridolin Wild, and Tjeerd olde Scheper, "Real-time auditory biofeedback system for learning a novel arm trajectory: a usability study." *Perspectives on Wearable Enhanced Learning (WELL) Current Trends, Research, and Practice*, pp. 385-409, (2019).

16- EV Isakova and Yu V Egorova, "Visual and acoustic feedback on the support reaction for upper and lower extremities: a case study of a female patient after a stroke." *Almanac of Clinical Medicine*, Vol. 49 (No. 6), pp. 435-42, (2021).

17- Katherine Hankinson, Alex Shaykevich, Ann-Maree Vallence, Jennifer Rodger, Michael Rosenberg, and Christopher Etherton-Beer, "A tailored music-motor therapy and real-time biofeedback mobile phone app ('GotRhythm') to promote rehabilitation following stroke: a pilot study." *Neuroscience Insights*, Vol. 17p. 26331055221100587, (2022).

18- Tormene Giorgino, Paolo Tormene, G Maggioni, Davide Capozzi, Silvana Quaglini, and C Pistarini, "Assessment of sensorized garments as a flexible support to self-administered post-stroke physical rehabilitation." *European Journal of Physical and Rehabilitation Medicine*, Vol. 45 (No. 1), pp. 75-84, (2009).

19- Chang-Yong Kim *et al.*, "Effect of spatial target reaching training based on visual biofeedback on the upper extremity function of hemiplegic stroke patients." *Journal of physical therapy science*, Vol. 27 (No. 4), pp. 1091-96, (2015).

20- Elizabeth B Brokaw, Emily Eckel, and Bambi R Brewer, "Usability evaluation of a kinematics focused Kinect therapy program for individuals with stroke." *Technology and Health Care*, Vol. 23 (No. 2), pp. 143-51, (2015).

21- Li-Fong Lin, Yi-Jia Lin, Zi-Hao Lin, Li-Yun Chuang, Wei-Chun Hsu, and Yuan-Hsiang Lin, "Feasibility and efficacy of wearable devices for upper limb rehabilitation in patients with chronic stroke: a randomized controlled pilot study." *European journal of physical and rehabilitation medicine*, Vol. 54 (No. 3), pp. 388-96, (2017).

22- Muhammed Nur Ögün, Ramazan Kurul, Mustafa Fatih Yaşar, Sule Aydin Turkoglu, Şebnem Avci, and Nebil Yildiz, "Effect of leap motion-based 3D immersive virtual reality usage on upper extremity function in ischemic stroke patients." *Arquivos de neuro-psiquiatria*, Vol. 77 (No. 10), pp. 681-88, (2019).

23- PK Paul, Ritam Chatterjee, Sucheta Chakraborty, KS Tiwary, PS Aithal, and S Sharma, "Advanced Healthcare Informatics Practice Vis-À-Vis Virtual Reality Implications—a Scientific Overview." *Immersive Virtual and Augmented Reality in Healthcare*, pp. 28-49, (2024).

24- Philémon Marcel-Millet, Philippe Gimenez, Alain Groslambert, Gilles Ravier, and Sidney Grospretre, "The type of visual biofeedback influences maximal handgrip strength and activation strategies." *European Journal of Applied Physiology*, Vol. 121pp. 1607-16, (2021).

25- Yusha Liu, Rafael ML Silva, Jeffrey B Friedrich, Dennis S Kao, Pierre D Mourad, and Aaron E Bunnell, "Surface electromyography-driven therapeutic gaming for rehabilitation of upper extremity weakness: a pilot study." *Plastic and reconstructive surgery*, Vol. 150 (No. 1), pp. 125-31, (2022).

26- Vivianne F Cardoso *et al.*, "Towards an upper limb rehabilitation tool after stroke based on surface electromyography biofeedback and virtual reality." *Research on Biomedical Engineering*, Vol. 38 (No. 3), pp. 1017-25, (2022).

27- Onur Armagan, Funda Tascioglu, and Cengiz Oner, "Electromyographic biofeedback in the treatment of the hemiplegic hand: a placebo-controlled study." *American Journal of Physical Medicine & Rehabilitation*, Vol. 82 (No. 11), pp. 856-61, (2003).

28- Steven L Wolf, "Electromyographic biofeedback applications to stroke patients: a critical review." *Physical therapy*, Vol. 63 (No. 9), pp. 1448-59, (1983).

29- Fatemeh Davarinia and Ali Maleki, "SSVEP-gated EMG-based decoding of elbow angle during goal-directed reaching movement." *Biomedical Signal Processing and Control*, Vol. 71p. 103222, (2022).

30- Liwei Cheng, Duanling Li, Gongjing Yu, Zhonghai Zhang, and Shuyue Yu, "Robotic arm control system based on brain-muscle mixed signals." *Biomedical Signal Processing and Control*, Vol. 77p. 103754, (2022).

31- Stephen L Toepp, Martin V Mohrenschildt, and Aimee J Nelson, "An EMG-Based Biofeedback System for Tailored Interventions Involving Distributed Muscles." *IEEE Sensors Journal*, (2023).

32- Juri Taborri *et al.*, "Feasibility of muscle synergy outcomes in clinics, robotics, and sports: a systematic review." *Applied bionics and biomechanics*, Vol. 2018 (No. 1), p. 3934698, (2018).

33- Vincent CK Cheung *et al.*, "Muscle synergy patterns as physiological markers of motor cortical damage."

Proceedings of the national academy of sciences, Vol. 109 (No. 36), pp. 14652-56, (2012).

34- Jenny C Castiblanco, Steffen Ortmann, Ivan F Mondragon, Catalina Alvarado-Rojas, Michael Jöbges, and Julian D Colorado, "Myoelectric pattern recognition of hand motions for stroke rehabilitation." *Biomedical Signal Processing and Control*, Vol. 57p. 101737, (2020).

35- Arsalan Asemi, Keivan Maghooli, Fereidoun Nowshiravan Rahatabad, and Hamid Azadeh, "Handwritten signatures verification based on arm and hand muscles synergy." *Biomedical Signal Processing and Control*, Vol. 76p. 103697, (2022).

36- Filip Gasparic *et al.*, "Nonlinear mapping from EMG to prosthesis closing velocity improves force control with EMG biofeedback." *IEEE Transactions on Haptics*, (2023).

37- Dario Farina, Roberto Merletti, and Roger M Enoka, "The extraction of neural strategies from the surface EMG." *Journal of applied physiology*, Vol. 96 (No. 4), pp. 1486-95, (2004).

38- Seyyed Ali Zendehbad, Hamid Reza Kobravi, Mohammad Mahdi Khalilzadeh, Athena Sharifi Razavi, and Payam Sasan Nezhad, "Presenting a New Muscle Synergy Analysis Based Mechanism to Design a Trackable Visual Biofeedback Signal: Applicable to Arm Movement Recovery After Ischemic Stroke." *IEEE Access*, Vol. 11pp. 70190-202, (2023).

39- Ali Zendehbad, Hamid Reza Kobravi, Mohammad Mahdi Khalilzadeh, Athena Sharifi Razavi, and Payam Sasannejad, "A New Visual Biofeedback Protocol Based on Analyzing the Muscle Synergy Patterns to Recover the Upper Limbs Movement in Ischemic Stroke Patients: A Pilot Study." *The Neuroscience Journal of Shefaye Khatam*, Vol. 11 (No. 3), pp. 11-24, (2023).

40- Seyedeh Somayeh Naghibi, Ali Fallah, Ali Maleki, and Farnaz Ghassemi, "Elbow angle generation during activities of daily living using a submovement prediction model." *Biological Cybernetics*, Vol. 114pp. 389-402, (2020).

41- Zonglei Chen, Minbo Ma, Tianrui Li, Hongjun Wang, and Chongshou Li, "Long sequence time-series forecasting with deep learning: A survey." *Information Fusion*, Vol. 97p. 101819, (2023).

42- Sabeen Ahmed, Ian E Nielsen, Aakash Tripathi, Shamoon Siddiqui, Ravi P Ramachandran, and Ghulam Rasool, "Transformers in time-series analysis: A tutorial." *Circuits, Systems, and Signal Processing*, Vol. 42 (No. 12), pp. 7433-66, (2023).

43- Siyuan Huang, Yepeng Liu, Fan Zhang, Yue Li, Jinjiang Li, and Caiming Zhang, "CrossWaveNet: A dual-channel network with deep cross-decomposition for Long-term Time Series Forecasting." *Expert Systems with Applications*, Vol. 238p. 121642, (2024).

44- Weiping Jiang, Jian Wang, Zhao Li, Wudong Li, and Peng Yuan, "A new deep self-attention neural network for GNSS coordinate time series prediction." *GPS Solutions*, Vol. 28 (No. 1), p. 3, (2024).

45- Roberto Merletti and PJJEK Di Torino, "Standards for reporting EMG data." *J Electromyogr Kinesiol*, Vol. 9 (No. 1), pp. 3-4, (1999).

46- Roberto Merletti, Marco Knaflitz, and Carlo J DeLuca, "Electrically evoked myoelectric signals." *Crit Rev Biomed Eng*, Vol. 19 (No. 4), pp. 293-340, (1992).

47- Roberto Merletti and Loredana R Lo Conte, "Surface EMG signal processing during isometric contractions." *Journal of Electromyography and Kinesiology*, Vol. 7 (No. 4), pp. 241-50, (1997).

48- Edward A Clancy and Neville Hogan, "Multiple site electromyograph amplitude estimation." *IEEE Transactions on Biomedical Engineering*, Vol. 42 (No. 2), pp. 203-11, (1995).

49- Claudio Orizio, Renza Perini, and Arsenio Veicsteinas, "Muscular sound and force relationship during isometric contraction in man." *European journal of applied physiology and occupational physiology*, Vol. 58pp. 528-33, (1989).

50- Carlo J De Luca, Alexander Adam, Robert Wotiz, L Donald Gilmore, and S Hamid Nawab, "Decomposition of surface EMG signals." *Journal of neurophysiology*, Vol. 96 (No. 3), pp. 1646-57, (2006).

51- Gabriel Rilling, Patrick Flandrin, and Paulo Goncalves, "On empirical mode decomposition and its algorithms." in *IEEE-EURASIP workshop on nonlinear signal and image processing*, (2003), Vol. 3 (No. 3): *Grado: IEEE*, pp. 8-11.

52- Yun Yang, ChongJun Fan, and HongLin Xiong, "A novel general-purpose hybrid model for time series forecasting." *Applied Intelligence*, Vol. 52 (No. 2), pp. 2212-23, (2022).

53- Konstantin Dragomiretskiy and Dominique Zosso, "Variational mode decomposition." *IEEE transactions on signal processing*, Vol. 62 (No. 3), pp. 531-44, (2013).

54- Mojtaba Nazari and Sayed Mahmoud Sakhaei, "Variational mode extraction: A new efficient method to derive respiratory signals from ECG." *IEEE journal of biomedical and health informatics*, Vol. 22 (No. 4), pp. 1059-67, (2017).

55- Qing Zhu, Fan Zhang, Shan Liu, Yiqiong Wu, and Lin Wang, "A hybrid VMD–BiGRU model for rubber futures time series forecasting." *Applied Soft Computing*, Vol. 84p. 105739, (2019).

56- Mojtaba Nazari and Sayed Mahmoud Sakhaei, "Successive variational mode decomposition." *Signal Processing*, Vol. 174p. 107610, (2020).

57- http://www.seniam.org/

58- David C Preston and Barbara E Shapiro, Electromyography and neuromuscular disorders e-book: clinical-electrophysiologic correlations (Expert Consult-Online). *Elsevier Health Sciences*, (2012).

59- Ce Zheng *et al.*, "Deep learning-based human pose estimation: A survey." *ACM Computing Surveys*, Vol. 56 (No. 1), pp. 1-37, (2023).

60- Tausif Diwan, G Anirudh, and Jitendra V Tembhurne, "Object detection using YOLO: Challenges, architectural successors, datasets and applications." *multimedia Tools and Applications*, Vol. 82 (No. 6), pp. 9243-75, (2023).

61- Muhammad Hussain, "YOLO-v1 to YOLO-v8, the rise of YOLO and its complementary nature toward digital manufacturing and industrial defect detection." *Machines*, Vol. 11 (No. 7), p. 677, (2023).

62- Nobuyasu Nakano *et al.*, "Evaluation of 3D markerless motion capture accuracy using OpenPose with multiple video cameras." *Frontiers in sports and active living*, Vol. 2p. 50, (2020).

63- Reuben Moyo, Stanley Ndebvu, Michael Zimba, and Jimmy Mbelwa, "A Video-based Detector for Suspicious Activity in Examination with OpenPose." *arXiv preprint arXiv:2307.11413*, (2023).

64- Dilliraj Ekambaram and Vijayakumar Ponnusamy, "Real-time AI-assisted visual exercise pose correctness during rehabilitation training for musculoskeletal disorder." *Journal of Real-Time Image Processing*, Vol. 21 (No. 1), p. 2, (2024).

65- Zhe Cao, Tomas Simon, Shih-En Wei, and Yaser Sheikh, "Realtime multi-person 2d pose estimation using part affinity fields." in *Proceedings of the IEEE conference on computer vision and pattern recognition*, (2017), pp. 7291-99.

66- Tomas Simon, Hanbyul Joo, Iain Matthews, and Yaser Sheikh, "Hand keypoint detection in single images using multiview bootstrapping." in *Proceedings of the IEEE conference on Computer Vision and Pattern Recognition*, (2017), pp. 1145-53.

67- Andrea d'Avella, Philippe Saltiel, and Emilio Bizzi, "Combinations of muscle synergies in the construction of a natural motor behavior." *Nature neuroscience*, Vol. 6 (No. 3), pp. 300-08, (2003).

68- Anh Huy Phan and Andrzej Cichocki, "Extended HALS algorithm for nonnegative Tucker decomposition and its applications for multiway analysis and classification." *Neurocomputing*, Vol. 74 (No. 11), pp. 1956-69, (2011).

69- Andrzej Cichocki, Rafal Zdunek, and Shun-ichi Amari, "Hierarchical ALS algorithms for nonnegative matrix and 3D tensor factorization." in *International conference on independent component analysis and signal separation*, (2007): *Springer*, pp. 169-76.

70- Yeongdae Kim, Sorawit Stapornchaisit, Hiroyuki Kambara, Natsue Yoshimura, and Yasuharu Koike, "Muscle Synergy and Musculoskeletal Model-Based Continuous Multi-Dimensional Estimation of Wrist and Hand Motions." *Journal of Healthcare Engineering*, Vol. 2020 (No. 1), p. 5451219, (2020).

71- Eugen Diaconescu, "The use of NARX neural networks to predict chaotic time series." *Wseas Transactions on computer research*, Vol. 3 (No. 3), pp. 182-91, (2008).

72- Georg Dorffner, "Neural networks for time series processing." *Neural network world*, Vol. 6 (No. 4), pp. 447-68, (1996).

73- Tsungnan Lin, Bill G Horne, Peter Tino, and C Lee Giles, "Learning long-term dependencies in NARX recurrent neural networks." *IEEE transactions on neural networks*, Vol. 7 (No. 6), pp. 1329-38, (1996).

74- Zachary C Lipton, John Berkowitz, and Charles Elkan, "A critical review of recurrent neural networks for sequence learning." *arXiv preprint arXiv:1506.00019*, (2015).

75- José Maria P Menezes Jr and Guilherme A Barreto, "Long-term time series prediction with the NARX network: An empirical evaluation." *Neurocomputing*, Vol. 71 (No. 16-18), pp. 3335-43, (2008).

76- Mike Schuster and Kuldip K Paliwal, "Bidirectional recurrent neural networks." *IEEE transactions on Signal Processing*, Vol. 45 (No. 11), pp. 2673-81, (1997).

77- Junyoung Chung, Caglar Gulcehre, KyungHyun Cho, and Yoshua Bengio, "Empirical evaluation of gated recurrent neural networks on sequence modeling." *arXiv preprint arXiv:1412.3555*, (2014).

78- Daoming She and Minping Jia, "A BiGRU method for remaining useful life prediction of machinery." *Measurement*, Vol. 167p. 108277, (2021).

79- Andrea d'Avella, Alessandro Portone, Laure Fernandez, and Francesco Lacquaniti, "Control of fast-reaching movements by muscle synergy combinations." *Journal of Neuroscience*, Vol. 26 (No. 30), pp. 7791-810, (2006).

80- Petre Stoica and Randolph L Moses, Spectral analysis of signals. *Pearson Prentice Hall Upper Saddle River, NJ*, (2005).

81- Tomoko Nemoto and David Beglar, "Likert-scale questionnaires." in *JALT 2013 conference proceedings*, (2014), pp. 1-8.

82- Shigeki Kubota *et al.*, "A newly developed upper limb single-joint HAL in a patient with elbow flexion reconstruction after traumatic brachial plexus injury: a case report." *Interdisciplinary Neurosurgery*, Vol. 10pp. 66-68, (2017).

83- Jiahao Chen and Hong Qiao, "Muscle-synergies-based neuromuscular control for motion learning and generalization of a musculoskeletal system." *IEEE Transactions on Systems, Man, and Cybernetics: Systems*, Vol. 51 (No. 6), pp. 3993-4006, (2020).

84- Richard A Schmidt, Timothy D Lee, Carolee Winstein, Gabriele Wulf, and Howard N Zelaznik, Motor control and learning: A behavioral emphasis. *Human kinetics*, (2018).

85- Seyed Safavynia, Gelsy Torres-Oviedo, and Lena Ting, "Muscle synergies: implications for clinical evaluation and rehabilitation of movement." *Topics in spinal cord injury rehabilitation*, Vol. 17 (No. 1), pp. 16-24, (2011).

86- Yoshua Bengio, Patrice Simard, and Paolo Frasconi, "Learning long-term dependencies with gradient descent is difficult." *IEEE transactions on neural networks*, Vol. 5 (No. 2), pp. 157-66, (1994).

87- Xiaolei Liu, Zi Lin, and Ziming Feng, "Short-term offshore wind speed forecast by seasonal ARIMA-A comparison against GRU and LSTM." *Energy*, Vol. 227p. 120492, (2021).

88- Navid Mohammadi Foumani, Lynn Miller, Chang Wei Tan, Geoffrey I Webb, Germain Forestier, and Mahsa Salehi, "Deep learning for time series classification and extrinsic regression: A current survey." *ACM Computing Surveys*, Vol. 56 (No. 9), pp. 1-45, (2024).